Thermal-Structural Analysis of a Square Solar Sail

Luisa Boni, Alessandro A. Quarta*, Giovanni Mengali

Department of Civil and Industrial Engineering, University of Pisa, I-56122, Italy

Abstract

The aim of this work is to improve an efficient methodology, recently developed to study the structural response of a classical square solar sails in free flight, under the action of the solar radiation pressure. The new approach models the effect of thermal loads acting on the sail's reflective surface. In particular, a square solar sail with a side length of 20 m at 1 au distance from the Sun is analyzed for different values of incidence and clock angles. The thermal-structural analyses are carried out under the assumption that the stress-displacement solution depends on the temperature field, but there is no inverse dependency. The thermal loads, for some attitude conditions, are shown to have remarkable effects on the sail deformation.

Keywords: square solar sail, thermal-structural analysis, FEM, scalloped sail configuration

1. Introduction

The availability of effective tools for structural analysis is a crucial point in the design of complex space structures. In this phase, the typical strategy is to use a numerical approach, based on a Finite Element (FE) analysis. However, in the context of space missions in which the primary propulsion system is a solar sail [1], the development of reliable FE models still remains a challenge, especially when compared to the design of a more conventional space structure. The recent success of the pionieristic Japanese mission IKAROS, in which a solar sail-based spacecraft had been successfully deployed in the interplanetary space [2, 3] for the first time, has demonstrated that this innovative propulsion concept, potentially able to grow the deep space mission scenarios [4, 5, 6, 7], is a feasible option during the preliminary mission design. In this context, the intrinsic characteristics of a solar sail configuration, such as its wide reflective surface with a very small thickness and the presence of long and slender stiffening booms [8, 9, 10], require the use of a strongly nonlinear analysis, which is made difficult by complex problems of numerical convergence.

An efficient methodology has been recently developed in Ref. [11] to study the structural response of a square solar sail in free flight, under the action of the solar radiation pressure. In particular, a square solar sail with a side length of 20 m, placed at a distance of 1 au from the Sun has been analyzed for different values of incidence (α) and clock (δ) angles. The methodology developed in Ref. [11] has been improved in Ref. [12], where the resultant forces acting on the spacecraft are calculated by taking into account the local curvature of each sail element in the evaluation of the solar pressure.

The aim of this work is to further refine such an analysis by introducing the effect of thermal loads acting on the sail reflective surface. So far, the latter aspect has been often overlooked, as a few research activities only deal with the structural effects of the temperature on solar sail behaviour. McInnes [13] defines the theoretical relationships necessary to evaluate the temperature of a flat solar sail for a given solar flux, solar angle, solar distance, and sail membrane optical properties. As an example of experimental activities carried out at NASA Glenn Research Center in 2004, the temperature of a flat sail quadrant is measured for different values of solar angles. In Refs. [14, 15], a numerical approach is used to study the effect of thermal

*Corresponding author

Email addresses: l.boni@dia.unipi.it (Luisa Boni), a.quarta@ing.unipi.it (Alessandro A. Quarta), g.mengali@ing.unipi.it (Giovanni Mengali)

Published in Acta Astronautica, Vol. 154 January 2019, pp. 268–277. doi: http://dx.doi.org/10.1016/j.actaastro.2018.03.037

loading on the sail surface. However, all of the previous works are based on the simplifying assumption that the only loading effect comes from a uniform temperature field acting on a flat sail membrane. Due to the out-of-plane deformation of the sail surfaces induced by the solar pressure, the sail membranes are not uniformly heated. In case of a non-uniformly heated membrane, Perrygo [16] predicts that the hotter regions sag less than the cooler regions, due to a non-zero Coefficient of Thermal Expansion (CTE). Accordingly, in Ref. [17], a non-uniform temperature distribution on a membrane specimen is experimentally determined and, in Ref. [18], a numerical effort is made to predict the influence of a non-uniform temperature field on the sail shape. Note that in Ref. [18], only the sail membrane sectors are modelled, while any interaction with booms and cables is neglected.

Recognizing these open issues, this paper takes into account the thermal-structural analysis of the whole solar sail structure and deals with the effects of both a uniform and non-uniform temperature distribution on the membranes. In particular, the sail configuration has five points of attachment with the booms, as is described in Ref. [11] and shown in Fig. 1.

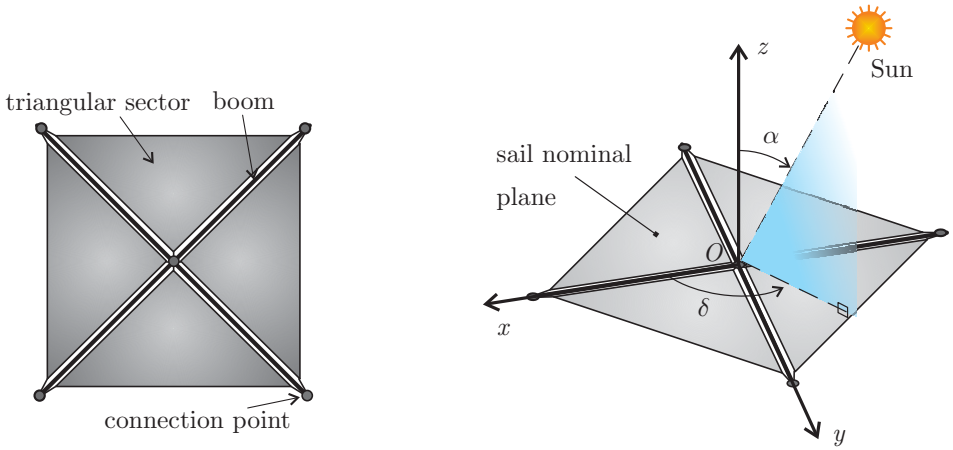

Figure 1: Solar sail configuration with five points of attachments (adapted from Ref. [11]).

2. Thermal-structural analyses: application to solar sails

A crucial phase for the solar sail structural design consists of performing a reliable thermal-structural analysis of the whole spacecraft when subjected to typical loading conditions. However, the reliability of such an analysis is determined by the accuracy with which the main loads acting on the structural components are evaluated, as well as by the effectiveness of the numerical approach used to simulate the loading conditions within an FE model. For these reasons, a thorough discussion of the adopted procedure is now presented.

2.1. Loading conditions

A thermal-structural analysis takes into account both mechanical and thermal loads. The mechanical loads here are considered the same as those described in Ref. [11], such as pre-tensioning, solar pressure at 1 au (calculated for different values of incidence, and clock angles), and inertial forces necessary to recover the equilibrium in free-flight conditions.

The temperature field acting on a solar sail is mainly induced by the thermal radiation in the outer space [17] which usually includes four contributions: solar thermal radiation, solar thermal radiation reflected by planets, infrared radiation of planets, and thermal radiation of vacuum in the universe. The solar thermal radiation is, however, the primary factor affecting the temperature on solar sails, while the other contributions can be neglected to a first order approximation [19]. Assuming a solar sail is orbiting at 1 au from the Sun, the solar irradiance is about $I \simeq 1360\,\mathrm{W/m^2}$. A specular reflectivity of the sail surface is assumed when considering both mechanical and thermal loads. In evaluating the temperature induced by the solar thermal radiation, the sail membrane is taken as opaque, in order to account for absorptivity

and reflectivity only, thus neglecting any amount of thermal energy transmitted through the membrane. Furthermore, a diffuse and grey emissivity of the sail surface is assumed, while any amount of dependence on radiation energy emitted on wavelength and direction is here neglected. The emissivity values are therefore assumed to be constant and averaged with respect to the infrared range, that is, the dominant range of wavelength [19]. The heat conduction through internal parts of the sail membrane is also taken into account in the evaluation of the equilibrium temperature.

As the heat absorbed by each surface portion depends on the local incidence angle of the solar rays, for a perfectly flat sail membrane the equilibrium temperature field is uniform over the whole surface, and its constant value varies with α. On the contrary, when the out-of-plane deformation of the sail membrane due to the action of the solar pressure is accounted for, each element of the surface is impinged at a different incidence angle $\alpha_{\rm el}$, depending on the local surface curvature. Therefore, a non-flat sail surface is characterized by a non-uniform temperature field. Furthermore, when $\alpha_{\rm el}$ is thought of as the sum of the incidence angle α plus an additional angle $\Delta\alpha_{\rm el}$ due to the loss of surface flatness, the thermal-structural analysis can be split, to a first order approximation, in two separated and sequential phases. The first one is related to the transition from the temperature $T_{\rm ext}$ in the vacuum (assumed equal to 3 K) to the uniform temperature T_α, and the second one is due to the local variation of temperature $(T_{\alpha+\Delta\alpha_{\rm el}} - T_\alpha)$. Note that T_α is calculated by assuming a flat surface, while $T_{\alpha+\Delta\alpha_{\rm el}}$ is associated to the deflected surface.

Since mechanical and thermal loads act simultaneously, due to the strong geometrical nonlinearity of the problem they should be considered simultaneously within the same analysis step. However, such an approach is not advisable due to the substantial difficulties in obtaining a numerical convergence, even in the presence of stabilization methods. To overcome such a problem, in the first analysis phase, only in-plane mechanical loads (i.e. pre-tensioning loads) are taken into account along with the heating from $T_{\rm ext}$ to T_α. The effect of the solar radiation pressure, and, consequently, the out-of-plane deformation induced on the sail surface, is considered in a second phase only, when the temperature varies from T_α to $T_{\alpha+\Delta\alpha_{\rm el}}$. Also, in the first analysis phase, only a uniform temperature field is associated with cables and boom, due to their negligible out-of-plane deformation.

2.2. Methodologies

The problem of thermal-stress analysis can be addressed by three different approaches of increasing complexity. The first one assumes that thermal and mechanical loads are fully uncoupled; the temperature field is independent of the stress-strain field and vice-versa. In the second approach, the stress-displacement solution depends on the temperature field but there is no inverse dependency. More precisely, a pure heat transfer problem is first solved and the results are then used as inputs for a stress analysis. However, even if the temperature can vary with time and position, it is not affected by the stress analysis solution. The third approach uses a fully coupled temperature-displacement procedure to simultaneously evaluate both stress-displacement and temperature fields. A fully coupled analysis is, however, computationally very onerous and is meaningful only when thermal and mechanical solutions are strongly coupled, as it happens in rapid metalworking processes. Therefore, this work uses the second approach to perform the thermal-structural analysis of a square solar sail. The heat transfer phase and the stress analysis have both been performed using software ABAQUS/STANDARD [20].

The first phase relative to the uniform component of the temperature field is made of one heat transfer analysis only, which provides the input for a succeeding stress analysis. At the end of this phase, all the solar sail components are in-plane deformed, according to their own heat transfer properties.

The second phase starts with an initial stress analysis applied to the solar sail geometry, taken as the output of the first phase. Only mechanical loads are considered in this analysis, which provides the first deflected configuration of the sail membrane. A heat transfer analysis is then performed on the out-of-plane deformed sail surface, thus providing a non-uniform temperature field, which is used as an input for a new stress analysis. Since a heat thermal analysis in ABAQUS requires the thermal radiation on a surface to be applied in the local normal direction only [20], the non-uniform heating has been simulated by applying non-uniform radiation intensities to each element on a flat geometry. The values of the radiation intensity are evaluated by means of an "ad hoc" Python script, which, while reading the output deformation from the stress analysis, elaborates the input thermal loads for the heat-transfer analysis. In the second stress analysis, in addition to mechanical loads, a local thermal stretching is induced by the transition from the uniform temperature T_α to the non-uniform $T_{\alpha+\Delta\alpha_{\rm el}}$. The mutual influence between the out-of-plane deformation

and the temperature field is thus modelled by iteratively performing the sequentially coupled heat transfer and stress analyses. The iterations of this methodology, adopted also in Ref. [18], are stopped when the variation of the maximum deflection of the sail membranes, W, is lower than 1% of the value relative to the mechanical loads alone, that is, W_{mec}. The iterative procedure is summarized in Fig. 2.

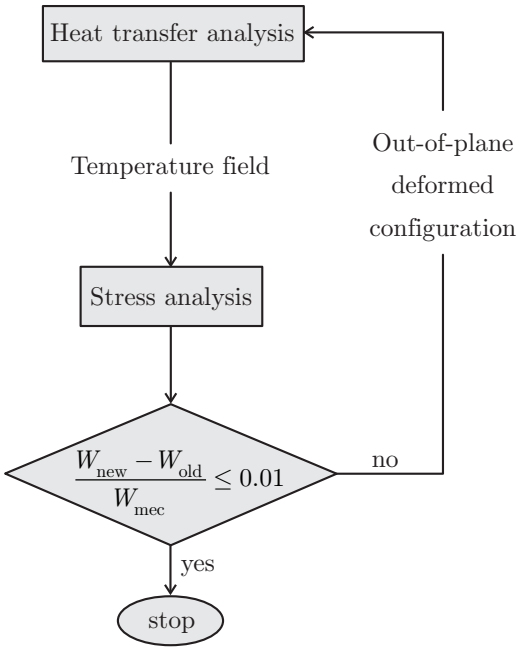

Figure 2: Iterative procedure for the thermal-structural analyses.

2.3. FE models

The model relevant to the stress analysis, described in Refs. [11, 12], uses elements with pure displacement degrees of freedom: S4 (four-node full integration shell element) for the sail membrane, B31 (two-node beam element) for the supporting boom, and T3D2 (2-node truss element) for the cables. The T3D2 element has been provided with "no-compression" behaviour, which makes the cables free of sagging, thus allowing a possible loss of pre-tensioning of the solar sail to be detected. The stress analysis consists of a two-step procedure, executed with these program settings: STATIC, GENERAL, Nlgeom=On, and Automatic Stabilization=None. In the first step a tensile pre-stress is applied to all cables as a PREDEFINED FIELD of TYPE=STRESS. The pre-stress (with a value of 2.35×10^7 N) on each cable induces a pre-tensioning field in the sail membrane, which causes a stress of about 1 Pa at each sector centre. In the second step, the solar pressure is applied as a SURFACE GENERAL TRACTION and the INERTIA RELIEF option is activated to model a body in a free flight condition. The main geometrical dimensions, characteristics, and the constituent material properties are reported in Tab. 1 for each component of the model.

The heat transfer study is performed by means of a single-step analysis of type HEAT TRANSFER with RESPONSE=STEADY STATE. The solar thermal radiation is applied as a SURFACE HEAT FLUX and, in the INTERACTION modulus, two separate conditions of SURFACE RADIATION to AMBIENT are enforced to the opposite sail membrane surfaces, accounting for their different emissivities. The model for the heat transfer analysis uses elements with pure thermal degrees of freedom consistent with the stress-displacement elements: the same number of nodes and integration points is required for the data transferring in the sequential procedure. Furthermore, the stress-displacement and thermal models are identically meshed, to obtain a high-precision assessment of the nodal temperatures. Figure 3 shows a typical mesh and the selected type of compatible elements.

Within ABAQUS software, SURFACE HEAT FLUX allows the solar thermal radiation to be applied on a given surface. This thermal load acts always normally to the surface, but the actual direction of the solar

Component	Boom	Cable	Control mast	Sail membrane
Material	composite	isotropic (Kevlar type)	isotropic	isotropic (Kapton type)
Section shape, radius [m]	tube circular, 0.229	solid circular, 0.0005	tube circular, 0.01705	N/A
Thickness [m]	7.5×10^{-6}	N/A	0.005	2.5×10^{-6}
Density [kg/m^3]	1908	1440	7660	1572
Elastic moduli [Pa]	$E_1 = 124 \times 10^9$	62×10^9	124×10^9	2.48×10^9
	$E_2 = 100 \times 10^9$			
	$E_3 = 100 \times 10^9$			
	$G_{12} = 47 \times 10^9$			
	$G_{13} = 38 \times 10^9$			
	$G_{23} = 46 \times 10^9$			
Poisson's ratio	$\nu_{12} = 0.3$	0.36	0.3	0.34
	$\nu_{13} = 0.3$			
	$\nu_{23} = 0.3$			

Table 1: Geometry and material properties of the solar sail components. Data adapted from Ref. [11].

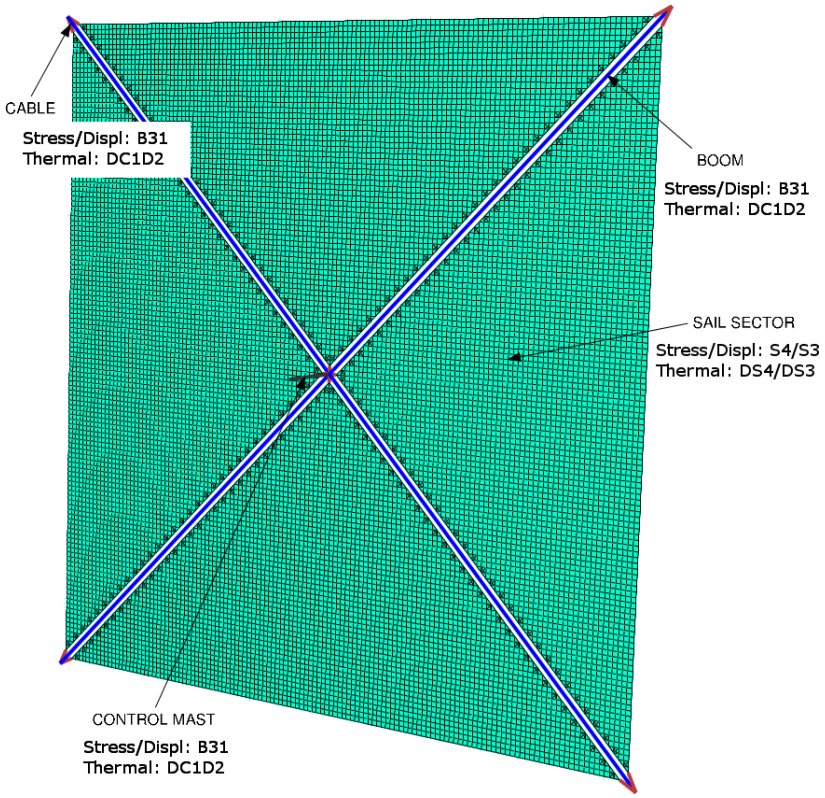

Figure 3: Mesh and element types.

rays (relative to the surface) cannot be assigned. Accordingly, the variation of the perceived heat radiation with the local surface curvature cannot be automatically accounted for. In this work, the problem has been solved by writing a Python script that first extracts the deformed shape of the sail from the stress analysis, and then uses it to calculate the orientation of each element. The same Python script evaluates the effective heat flux perceived by each element by calculating the projection of the heat radiation vector on the local normal, and launches a thermal analysis on a undeformed sail configuration subjected to a non-uniform heat flux on the elements.

3. Uniform temperature field: effects and design considerations

On a perfectly flat solar sail configuration, the temperature of each spacecraft component, starting from T_{ext}, reaches a constant value, depending on the incidence angle α and on the heat transfer properties of the specific structural member, see Tab. 2.

Components	Absorptivity	Emissivity	Conductivity (Wm/K)
Sail membrane (sun-side)	0.1	0.03	0.12
Sail membrane	0.2	0.34	0.12
Booms	0.91	0.83	0.79
Cables	0.47	0.85	0.04

Table 2: Heat transfer properties of the solar sail components.

The highest temperature induced by the solar radiation, which occurs at $\alpha = 0\,\text{deg}$, is about $11\,^{\circ}\text{C}$ for the sail membrane (made of Kapton [11]), $12.5\,^{\circ}\text{C}$ for the cables (made of Kevlar [11]) and $67\,^{\circ}\text{C}$ for the booms (made of special composite material [11]). In the stress analysis and in the presence of a pre-tensioning mechanical load only, each component expands or shrinks (for negative CTE), according to its temperature variation and CTE value, see Tab. 3.

Components	CTE (ppm/K)
Sail membrane	20
Booms	-2.5
Cables	-0.41

Table 3: CTE values of the solar sail components.

As the CTE of the booms is almost zero and the CTE of Kapton is one order of magnitude greater than that of the cable, the latter sags and a loss of pre-tensioning occurs. In particular, the negative CTE value of Kevlar induces a shrink of the cables that cannot compensate the membrane enlargement to maintain the pre-tensioning. Such an effect, described also in Ref. [14], indicates the need of employing a system for pre-tensioning recovery. Figure 4 illustrates how the deformed shape of the solar sail components is superimposed to the undeformed configuration. The same figure also shows a clear decrease of the angle between the cable direction and the internal edge of the sail sector. An important result of this analysis is the proof of a negligible out-of-plane deflection of the sail, which strengthens the assumption of separating the thermal-structural study in two distinct and sequential phases: the first one dominated by in-plane deformations and the second one by out-of-plane deflections.

4. Non-uniform temperature field: effects and design considerations

The effects of a non-uniform temperature field are studied using the solar sail geometrical configuration that results from the previous analysis (Fig. 4). Furthermore, the pre-stress conditions are assumed to be recovered by applying the original tension loads to the cables. Because the pre-tensioning loads act in a different direction with respect to the mid-line of the sail sectors, the pre-stress field induced on the sail membrane is varied.

The results of the iterative procedure described in Fig. 2 show that, assuming for example $\alpha = 0\,\text{deg}$, the induced thermal gradients are so small that after one iteration only the convergence criterion is satisfied, i.e., the maximum sail deflection varies less than 1% of the initial value. The non-uniform temperature field introduced by the out-of-plane sail deformation, see Fig. 5, is on the order of $10^3\,^{\circ}\text{C}$ and is not sufficient for appreciably modifying the sail condition after the uniform heating. The final value of the sail maximum deflection, see Fig. 6, is about 22% greater than that calculated in Refs. [11, 12] since the sail surface is larger due to the uniform heating, and the pre-tensioning field is less effective. This means, if the solar rays

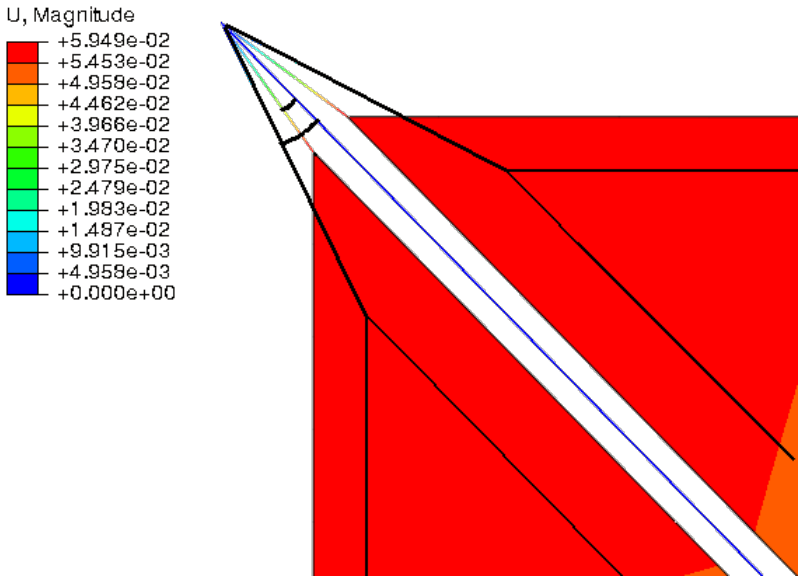

Figure 4: Deformation of the solar sail components due to uniform temperature fields.

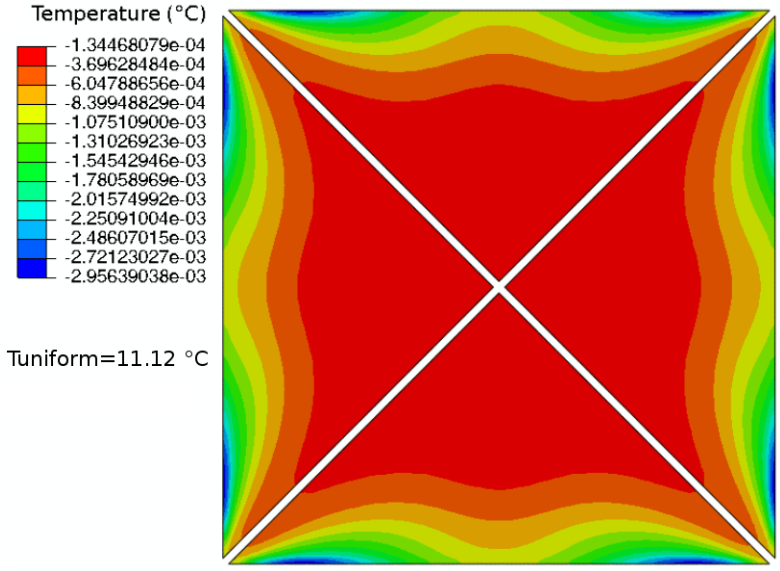

Figure 5: Non-uniform temperature field for $\alpha = 0\,\text{deg}$.

impinge on the sail reference surface at a right angle, the only remarkable effect of the thermal loads results from the uniform part of the field temperature.

The situation relative to a greater value of the incidence angle, for example $\alpha = 35\,\text{deg}$ (the value of α that maximizes the tangential sail force component), is more complex. In fact, when the angle of incidence increases, for each of the considered values of the clock angle ($\delta = \{0, 45, 90\}\,\text{deg}$), the initial value of the maximum sail deflection is about 25% greater than that predicted in Refs. [11, 12] by a pure stress analysis. By going on with the iterative procedure, the thermal gradients produce, at the free edges of the solar sail, remarkable out-of-plane deformations. Such deformations in the first iteration occur as mild corrugations on one or two (depending on the value of the clock angle) of the free edges of the sail. These corrugations,

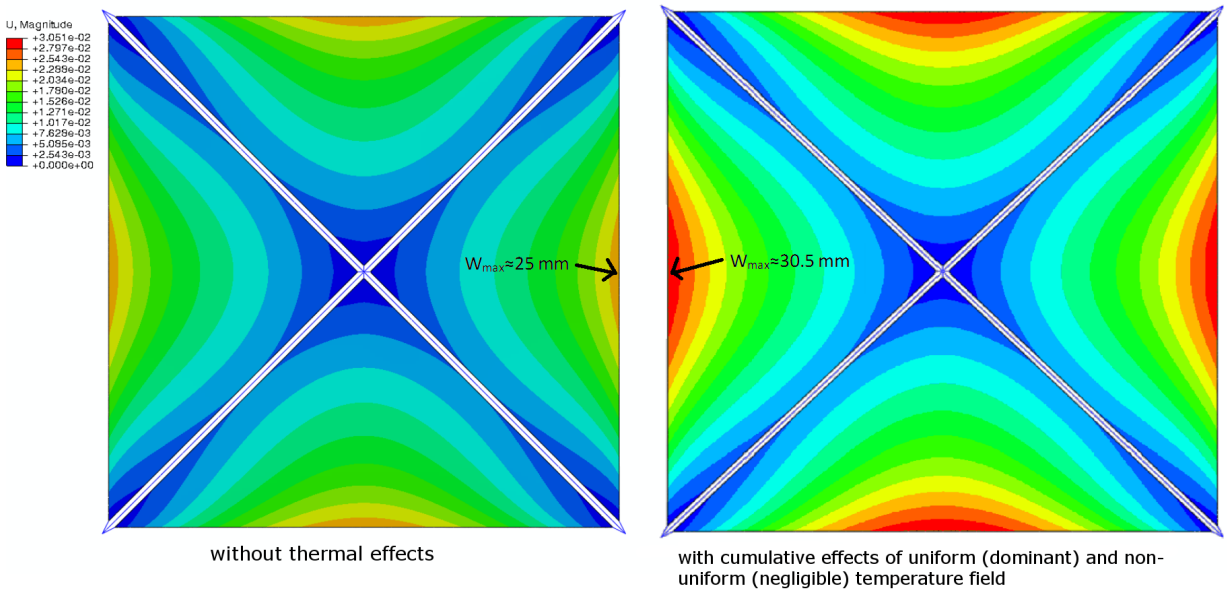

Figure 6: Effect of temperature on the sail out-of-plane displacements for $\alpha = 0\,\text{deg}$.

albeit quite localized, tend to become deeper and originate sharp wrinkles when the iterations increase, as is shown in Fig. 7 which illustrates the situation at the end of the fifth iteration. A synoptic illustration of the results is given in Fig. 7 to represent the variation of the out-of-plane displacement field from an ideal case to a situation with both uniform and non-uniform temperature on the sail surface. To complete the thermal load analysis, the out-of-plane displacements along the horizontal median of the most deformed sail sector is reported in Fig. 8, in the worst case of $\alpha = 35\,\text{deg}$ and $\delta = 45\,\text{deg}$. The non-uniform temperature field at the fifth iteration is shown in Fig. 9.

The described behaviour prevents the procedure from the achievement of a given convergence criterion. Even if the majority of the sail surface is not affected by such wrinkles (and therefore it reaches an equilibrium condition), in some localized regions the deformations become unstable and cause a loss of numerical convergence. This problem is described also in Ref. [18], where it is partially solved by varying the convergence criterion. In particular, in Ref. [18] the root-mean-squared (RMS) difference between new and old nodal positions is evaluated on the whole sail surface and, as long as it is greater than 1% of the initial maximum sail deflection, the shape model continues iterating between the sail temperature and the sail geometry. In this paper, the iteration is chosen to be continued until a numerical convergence is lost rather than stopping it before the fulfilment of a modified criterion. In Fig. 7, the reported results are relative to the last iteration (the fifth one) when a numerical convergence was achieved.

In conclusion, for increasing values of the incidence angle, both the uniform and non-uniform parts of the temperature fields produce significant effects which must be taken into account in the design phase of a solar sail. The thermal loads can cause the loss of both pre-tensioning (uniform temperature field) and rotational equilibrium due to the asymmetrical wrinkles on the surface introduced by the non-uniform heating. To avoid or at least reduce the detrimental effects of the thermal loads, the solar sail should be equipped with an attitude control system that includes a flatness control, such as the shifted panels method [21] which is capable of recovering both pre-tensioning and attitude stability.

During the analysis, the effect of an increasing size of the solar sail has been investigated. As far as the uniform temperature field is concerned, the increase of the sail membrane area, which is proportional to the square of the sail side, is more effective in terms of obtained thrust. The unavoidable loss of pre-tensioning is therefore more insidious to recover, since the change of direction of the pre-tensioning forces tends to reduce the effectiveness of the pre-stress field. An increase of sail size tends to induce the problem of thermal wrinkles due to the non-uniform temperature field. As a matter of fact, such a phenomenon is due to the

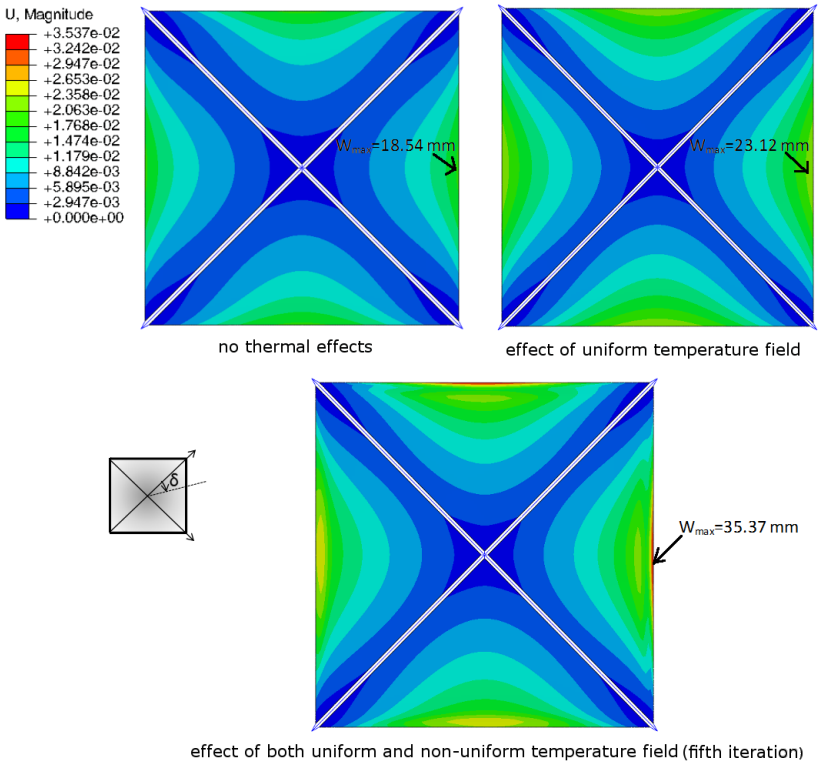

(a) $\alpha = 35\,\text{deg}$ and $\delta = 0\,\text{deg}$

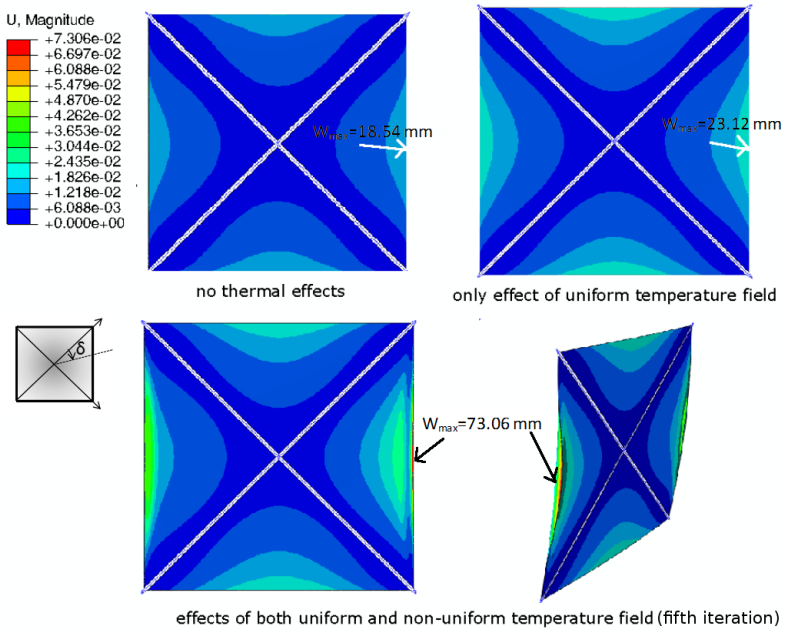

(b) $\alpha = 35\,\text{deg}$ and $\delta = 45\,\text{deg}$ (worst case)

Figure 7: Evolution of the out-of-plane displacements for effect of temperature.

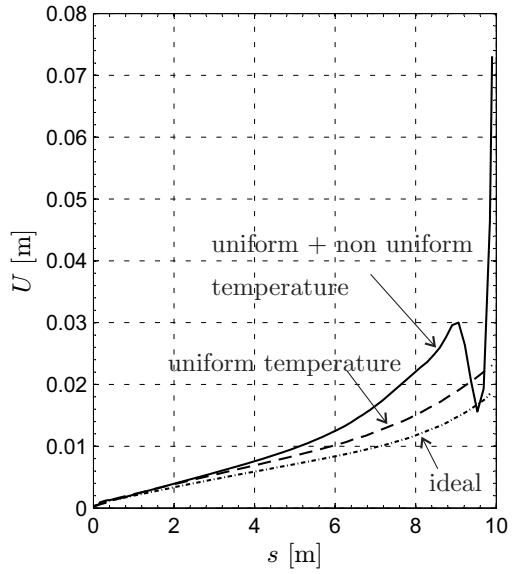

Figure 8: Out-of-plane displacements along the sector median for $\alpha = 35\,\text{deg}$ and $\delta = 45\,\text{deg}$.

interaction between the local change of curvature of the sail surface and a non-zero angle of incidence of the solar rays. From a numerical viewpoint, such a behavior causes an early loss of convergence.

Another approach useful for mitigating or even eliminating the thermal induced wrinkles, which are localized at the sail free edges, consists of varying the shape of the sail sectors. This is possible by introducing a scalloped shape of the external sail edges which "cuts-off" the regions affected by the stronger thermal gradients. Solar sails with a scallop factor (defined as the ratio between the area of the scalloped to the non-scalloped sail) of 75% are of common use [22] since, when associated with rigid edge support chords [23], the uniformity of the membrane stress field is optimized and a high quality of sail deployment can be achieved. To better investigate such a solution, all the thermal-structural analyses have been repeated on a solar sail with a scallop factor of 75%.

5. Scalloped solar sail

The ideal design of a solar sail should produce a sail membrane with a "wrinkle free" thrust area. Such a result may be obtained by means of curved edges with chords which allow the sail membrane to be stressed in an isotropic way. Another characteristic that has promoted the adoption of a scalloped configuration is the higher resistance of the sail membrane to gravity during ground testing, due to the substantial reduction of draping.

According to Ref. [23], if a scallop is very shallow, the chord loading required for the sail pre-tensioning is large and the structural booms are quite stressed in compression. In order to reduce the loads acting on chord and booms, it would be desirable to increase the scallop depth. Unfortunately, a higher scallop depth corresponds to a lower thrust area and therefore the solar sail has to be scaled up to recover the original propulsive performance. Furthermore, together with the sail membrane, the masts must become longer and, consequently, heavier. As discussed in Refs. [22, 23], a good trade-off value is represented by a configuration with a scallop factor of 75%. Accordingly, a value of the scallop factor of 75% has been assumed in this work (without the presence of perimetric chords) to study the influence of a geometric variation of solar sail edges on the response to thermal-structural loads.

5.1. FE models

The model with a scalloped solar sail has been obtained by cutting-off circular segments from the sail free edges. The radius of the circular segments has been chosen such as to cut-off 25% of the original sail surface. The meshing criteria for the scalloped sail sectors are definitively more critical than those for triangular

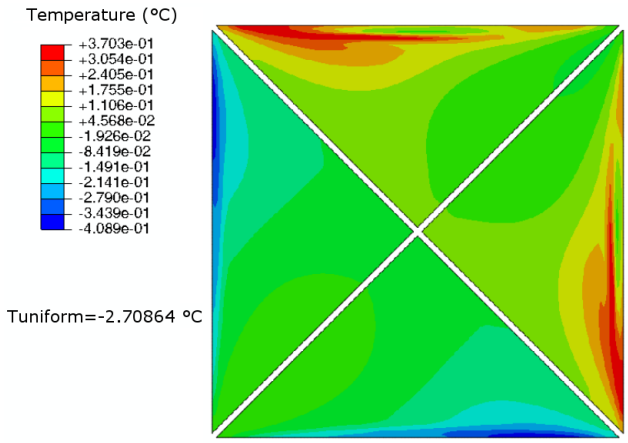

(a) $\alpha = 35\,\text{deg}$ and $\delta = 0\,\text{deg}$

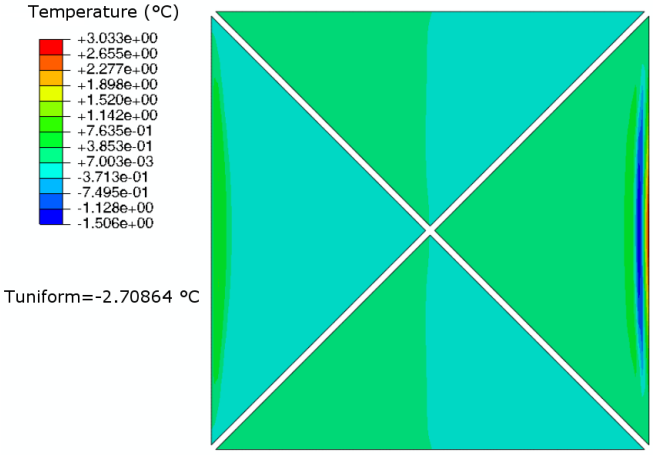

(b) $\alpha = 35\,\text{deg}$ and $\delta = 45\,\text{deg}$ (worst case)

Figure 9: Non-uniform temperature field at fifth iteration.

sectors since the curvature of the external edges causes local bad performance of S4 elements in terms of aspect-ratio, skewness and warping. To avoid an excessive deformation of the elements and difficulties in the numerical convergence with poor quality of the results, the S4 elements have been replaced by S3 elements in certain critical regions. Triangular elements, despite their excessive stiffness, give better performance in areas with high curvature. In particular, the classic tests to estimate the degree of deformation of the S4 elements in the regions near the free edges give poor results both in terms of aspect-ratio and skewness [20]. Such a low quality of the mesh in regions previously identified as very critical for the occurrence of thermal wrinkles is not acceptable. As a consequence, S4 elements have been used in central square regions covering about 80% of the sail surface, while in the remaining external zones S3 elements have been adopted. In addition, the over-stiffness of the triangular elements has been mitigated by further decreasing their mean size. A typical mesh is shown in Fig. 10.

5.2. Uniform temperature field

Similar to the case of straight edges, the cables sag, a loss of pre-tensioning occurs, and the angle between the cable direction and the internal edge of the sail sector decreases. Scalloped solar sails also require a system for pre-tensioning recovery.

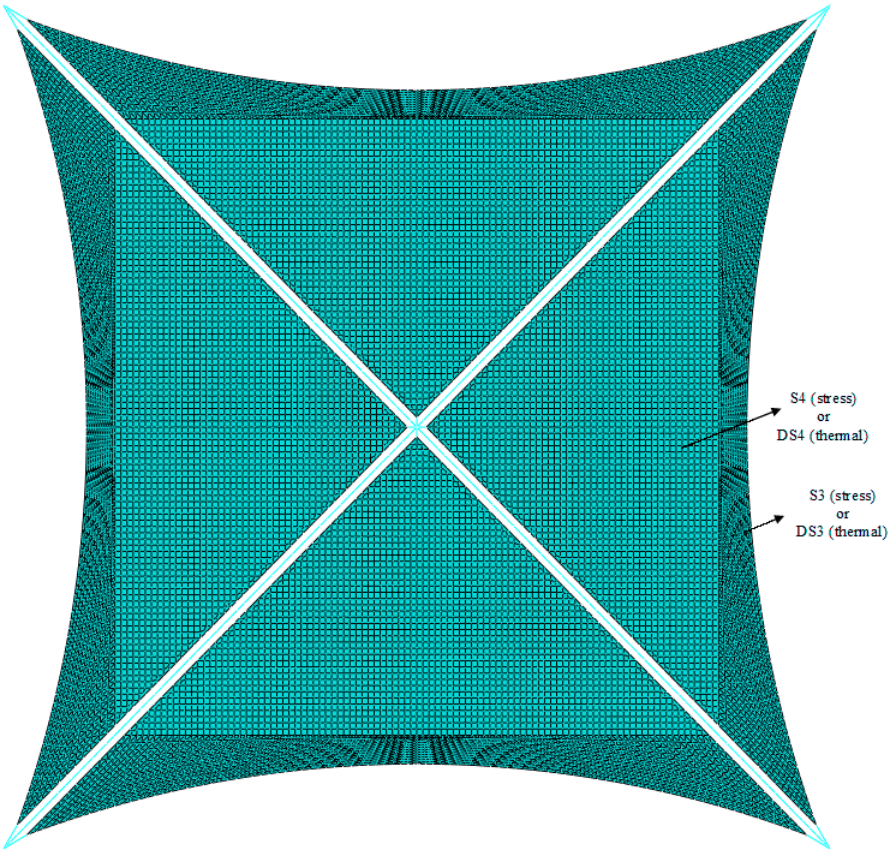

Figure 10: Mesh of the scalloped solar sail: about 83% of quadrilateral elements and remaining triangular elements.

5.3. Non-uniform temperature field

As for the model with straight edges, the recovery of the pre-stress field in the sail membrane is obtained by applying the same value of tension to the cables. The pre-stress distribution on the sail sector is modified due to the change of direction of the cable forces, and this variation is more pronounced than for a non-scalloped sail. As a consequence, the pre-tensioning is less effective in avoiding too large sail deflections, and the numerical convergence performance reduces, due to an increase of regions in compression. The scalloped solar sails are always supplied with perimetric rigid chords and interposed compliant borders [23] which allow the uniformity of the pre-stress field to be optimized and less sensitive to the cable orientation. However, the modelling of such a complex system is beyond the scope of this paper.

The maximum deflection of the sail membrane at the beginning of numerical iterations is about 17% greater than the value calculated in the presence of mechanical loads alone due to the surface enlargement induced by the uniform heating and to the variation of the pre-tensioning pattern. The obtained results indicate that despite a small decrease in the resultant force due to the lower area (with a reduction of 25%), the introduction of the scalloped shape is able to solve the problem of locally unstable thermal wrinkles with a numerical convergence obtained in a few iterations, see Fig. 11. The results are shown, to highlight the progressive thermal effects, for no temperature case, and for only uniform temperature and, finally, for both uniform and non-uniform temperature of the sail surface. The out-of-plane displacement along the horizontal sector median are represented for the worst case of $\alpha = 35\,\text{deg}$ and $\delta = 45\,\text{deg}$ in Fig. 12. The non-uniform temperature field are shown in Fig. 13.

The scalloped shape of the square solar sail is thus able to avoid the detrimental effects of the non-uniform component of the temperature field, but such a configuration must use a suitable system for controlling the sail pre-tensioning.

6. Conclusions

A procedure has been discussed for the preliminary design of a classical square solar sail, which takes into account both the main mechanical and thermal loads acting on the whole solar sail structure. The methodology is based on the finite element analyses performed with the aid of a commercial software but due to its iterative nature is coupled and managed by means of specific Python codes. The results show a remarkable influence of the thermal loads on the solar sail performance, and the conclusion is that they cannot be neglected also in the preliminary phase of the design process. According to the different kinds of thermal-structural phenomena identified by the present study, some recommended design solutions have been identified, such as the introduction of an attitude control system with a suitable flatness control and the use of a scalloped shaped sail sectors.

References

[1] B. Fu, E. Sperber, F. Eke, Solar sail technology–a state of the art review, Progress in Aerospace Sciences 86 (2016) 1–19 .

[2] Y. Tsuda, O. Mori, R. Funase, et al., Achievement of IKAROS - japanese deep space solar sail demonstration mission, Acta Astronautica 82 (2013) 183–188, doi: 10.1016/j.actaastro.2012.03.032.

[3] Y. Tsuda, O. Mori, R. Funase, et al., Flight status of IKAROS deep space solar sail demonstrator, Acta Astronautica 69 (9-10) (2011) 833–840, doi: 10.1016/j.actaastro.2011.06.005.

[4] I. Dandouras, B. Pirard, J. Y. Prado, High performance solar sails for linear trajectories and heliostationary missions, Advances in Space Research 34 (1) (2004) 198–203 .

[5] A. A. Quarta, G. Mengali, Semi-analytical method for the analysis of solar sail heliocentric orbit raising, Journal of Guidance, Control, and Dynamics 35 (1) (2012) 330–335, doi: 10.2514/1.55101.

[6] G. Mengali, A. A. Quarta, Optimal heliostationary missions of high-performance sailcraft, Acta Astronautica 60 (8-9) (2007) 676–683, doi: 10.1016/j.actaastro.2006.07.018.

[7] A. A. Quarta, G. Mengali, Solar sail missions to mercury with venus gravity assist, Acta Astronautica 65 (3–4) (2009) 495–506, doi: 10.1016/j.actaastro.2009.02.007.

[8] G. Vulpetti, C. Circi, Mass breakdown model of solar-photon sail shuttle: The case for mars, Acta Astronautica 119 (2016) 87–100, doi: 10.1016/j.actaastro.2015.11.010.

[9] J. Block, M. Straubel, M. Wiedemann, Ultralight deployable booms for solar sails and other large gossamer structures in space, Acta Astronautica 68 (7-8) (2011) 984–992, doi: 10.1016/j.actaastro.2010.09.005.

[10] C. Sickinger, L. Herbeck, E. Breitbach, Structural engineering on deployable CFRP booms for a solar propelled sailcraft, Acta Astronautica 58 (4) (2006) 185–196, doi: 10.1016/j.actaastro.2005.09.011.

[11] L. Boni, G. Mengali, A. A. Quarta, Solar sail structural analysis via improved finite element modeling, Proceedings of the Institution of Mechanical Engineers, Part G: Journal of Aerospace Engineering 231 (2) (2017) 306–318, doi: 10.1177/0954410016636164.

[12] L. Boni, G. Mengali, A. A. Quarta, Finite element analysis of solar sail force model with mission application, In press. Proceedings of the Institution of Mechanical Engineers, Part G: Journal of Aerospace Engineering .

[13] C. R. McInnes, Solar Sailing: Technology, Dynamics and Mission Applications, Springer-Praxis Series in Space Science and Technology, Springer-Verlag, Berlin, 1999, pp. 47–49.

[14] R. B. Malla, C. Lin, Structural dynamic response of a square solar sail under solar pressure and thermal loading, in: Ninth Biennial Conference on Engineering, Construction, and Operations in Challenging Environments, League City (Houston), March 7–10, 2004, doi: 10.1061/40722(153)134.

[15] J. Zheng, Z. Sheng, H. Zhou, W. Huang, L. Sheng, Structural analysis about a new solar sail, Chinese Journal of Space Science 29 (2) (2009) 249–256, doi: 10.11728/cjss2009.02.249.

[16] C. Perrygo, Gossamer Spacecraft: Membrane And Inflatable Structures Technology For Space Applications, Progress in Astronautics and Aeronautics, American Institute of Aeronautics and Astronautics, 2001, Ch. 20, pp. 503–526, ISBN: 978-1-56347-403-3.

[17] J. J. Miles, J. R. Blandino, C. H. R. Jenkins, R. S. Pappa, J. Banik, H. Brown, K. McEvoy, Evaluation of microbolometer-based thermography for gossamer space structures, in: Proceedings of Optics and Photonics 2005, SPIE, San Diego (California), July 31–August 4, 2005, doi: 10.1117/12.618069.

[18] J. Banik, P. Lively, B. Taleghani, C. H. Jenkins, Solar sail topology variations due to on-orbit thermal effects, Journal of Spacecraft and Rockets 44 (3) (2007) 558–570, doi: 10.2514/1.22902.

[19] Y. A. Cengel, Heat Transfer: A Practical Approach, 2nd Edition, Mcgraw-Hill, 2002, pp. 561–599, ISBN: 978-0071151504.

[20] Dassault Systèmes, Abaqus 6.11 Analysis User's Manual - Volume II: Analysis, DCS Simulia (2011).

[21] B. Fu, F. O. Eke, Attitude control methodology for large solar sails, Journal of Guidance, Control, and Dynamics 38 (4) (2015) 662–670, doi: 10.2514/1.G000048.

[22] D. Murphy, T. Trautt, M. McEachen, D. Messner, G. Laue, P. Gierow, Progress and plans for system demonstration of a scalable square solar sail, in: 14th AAS/AIAA Space Flight Mechanics Conference, Maui (Hawaii), February 8–12, 2004, paper AAS 04-105.

[23] M. Mikulas, A. Adler, Rapid structural assessment approach for square solar sails including edge support cords, in: 44th AIAA/ASME/ASCE/AHS/ASC Structures, Structural Dynamics, and Materials Conference, Norfolk (Virginia), April 7–10, 2003, doi: 10.2514/6.2003-1447.

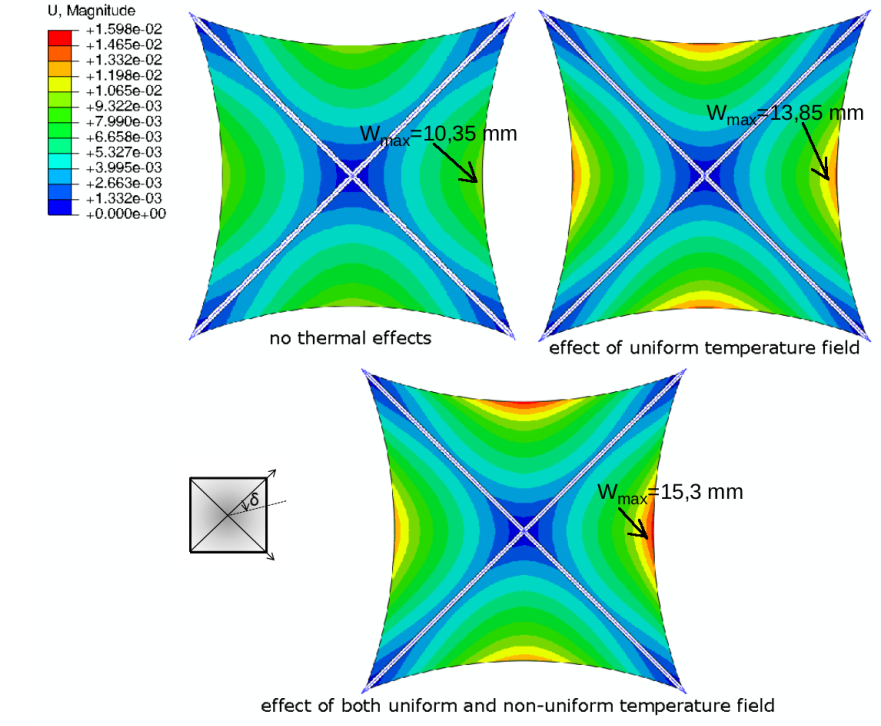

(a) $\alpha = 35\,\text{deg}$ and $\delta = 0\,\text{deg}$

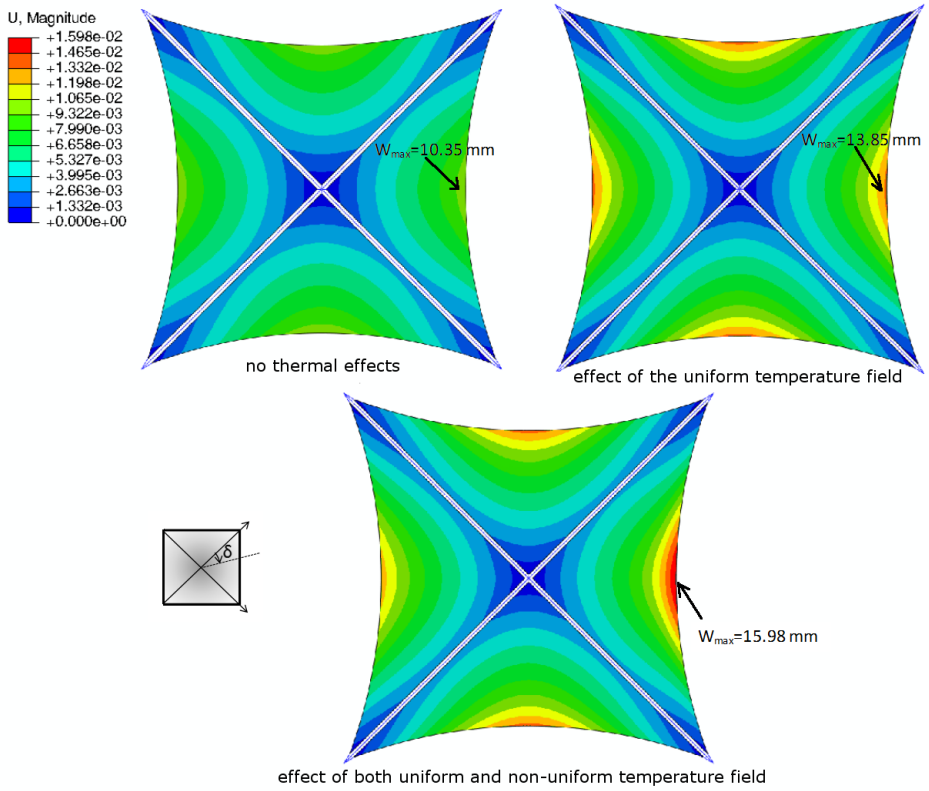

(b) $\alpha = 35\,\text{deg}$ and $\delta = 45\,\text{deg}$ (worst case)

Figure 11: Evolution of the out-of-plane displacements due to the temperature after numerical convergence with a scallop of 75%.

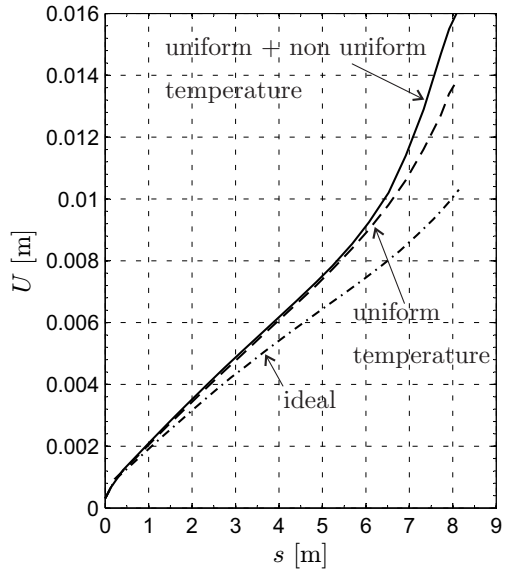

Figure 12: Out-of-plane displacements along the sector median for $\alpha = 35\,\text{deg}$ and $\delta = 45\,\text{deg}$ with a scallop of 75%.

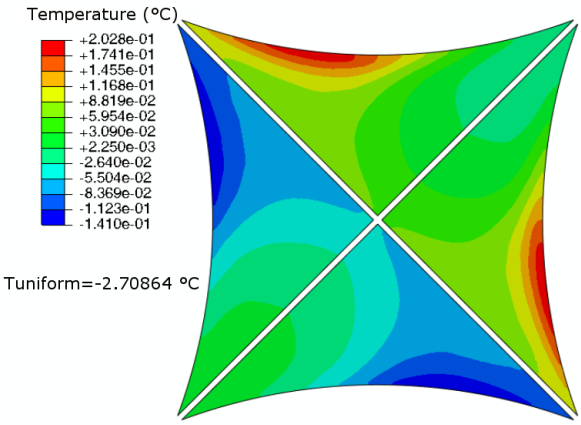

(a) $\alpha = 35\,\text{deg}$ and $\delta = 0\,\text{deg}$

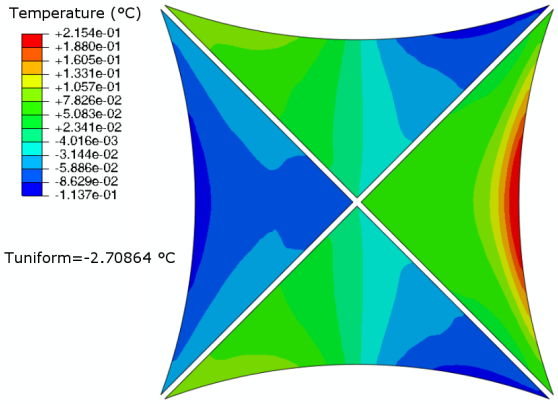

(b) $\alpha = 35\,\text{deg}$ and $\delta = 45\,\text{deg}$ (worst case)

Figure 13: Non-uniform temperature field with a scallop of 75% at numerical convergence.